ACS APPLIED MATERIALS & INTERFACES

www.acsami.org

Research Article

Realizing 22.3% EQE and 7-Fold Lifetime Enhancement in QLEDs via Blending Polymer TFB and Cross-Linkable Small Molecules for a Solvent-Resistant Hole Transport Layer

Pengyu Tang,[‖] Liming Xie,[‖] Xueying Xiong, Changting Wei, Wenchao Zhao, Ming Chen, Jinyong Zhuang,* Wenming Su,* and Zheng Cui

Cite This: *ACS Appl. Mater. Interfaces* 2020, 12, 13087−13095

Read Online

ACCESS | Metrics & More | Article Recommendations | Supporting Information

ABSTRACT: Poly[(9,9-dioctylfluorenyl-2,7-diyl)-*alt*(4,4′-(*N*-(4-butylphenyl)))] (TFB) has been widely used as a hole transport layer (HTL) material in cadmium-based quantum dot light-emitting diodes (QLEDs) because of its high hole mobility. However, as the highest occupied molecular orbital (HOMO) energy level of TFB is −5.4 eV, the hole injection from TFB to the quantum dot (QD) layer is higher than 1.5 eV. Such a high oxidation potential at the QD/HTL interface may seriously degrade the device lifetime. In addition, TFB is not resistant to most solvents, which limits its application in inkjet-printed QLED display. In this study, the blended HTL consisting of TFB and cross-linkable small molecular 4,4′-bis(3-vinyl-9*H*-carbazol-9-yl)-1,1′-biphenyl (CBP-V) was introduced into red QLEDs because of the deep HOMO energy level of CBP-V (−6.2 eV). Compared with the TFB-only devices, the external quantum efficiency (EQE) of devices with the blended HTL improved from 15.9 to 22.3% without the increase of turn-on voltage for spin-coating-fabricated devices. Furthermore, the blended HTL prolonged the T90 and T70 lifetime from 5.4 and 31.1 to 39.4 and 148.9 h, respectively. These enhancements in lifetime are attributed to the low hole-injection barrier at the HTL/QD interface and high thermal stability of the blended HTL after cross-linking. Moreover, the cross-linked blended HTL showed excellent solvent resistance after cross-linking, and the EQE of the inkjet-printed red QLEDs reached 16.9%.

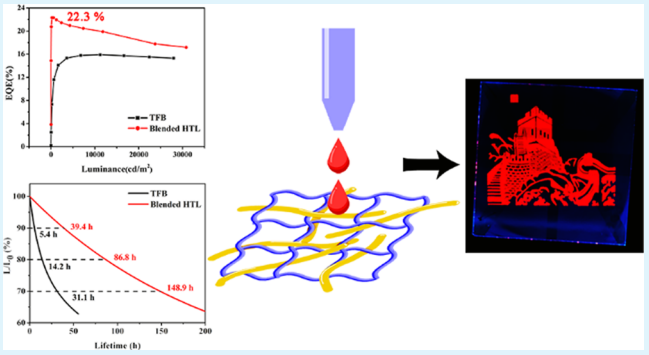

KEYWORDS: *quantum dot light-emitting diodes, blended HTL, solvent resistance, inkjet printing, charge balance*

INTRODUCTION

Light-emitting diodes based on colloidal quantum dots (QLEDs) are poised to be the next-generation display technology because of their unique features of self-emitting, pure emission color, easy fabrication, and high photostability.[1−17] With the continuous exploration and research into device physics and material chemistry, cadmium-based quantum dots (QDs) have reached the commercial standard in terms of material stability and quantum yield.

It is known that hole mobility is lower than that of the electron in cadmium-based QLEDs.[7] Poly[(9,9-dioctylfluorenyl-2,7-diyl)-*alt*(4,4′-(*N*-(4-butylphenyl)))] (TFB) is a commonly used polymer hole transport material (HTM) with higher mobility[18] (∼10^{-3} cm^2 V^{-1} s^{-1}) than other HTMs. The red QLEDs employing TFB as the HTL have shown good performance in the literature with a low turn-on voltage (1.8 V) and high external quantum efficiency (EQE) (>20%).[19−21] However, the low HOMO level (∼−5.4 eV) of TFB causes the problems of hole injection from the HTL to QD layer and high oxidation potential at the HTL/QD interface because of the large injection barrier (∼1.5 eV) at the interface.

Recent studies on OLEDs and QLEDs have indicated that double or blended HTL structures with a stepwise HOMO energy-level alignment could benefit the hole transport at interfaces.[22−27] Among them, the blended structure is simpler than the double structure in terms of solvent processes such as spin-coating.

In solution processes, orthogonal solvent systems[28−30] are commonly used to handle the problem of interfacial erosion. Such systems are, however, difficult to apply to the inkjet printing process[31] because the surface tension and viscosity of solvents must be taken into consideration for the inks to be

Received: January 17, 2020
Accepted: February 24, 2020
Published: February 24, 2020

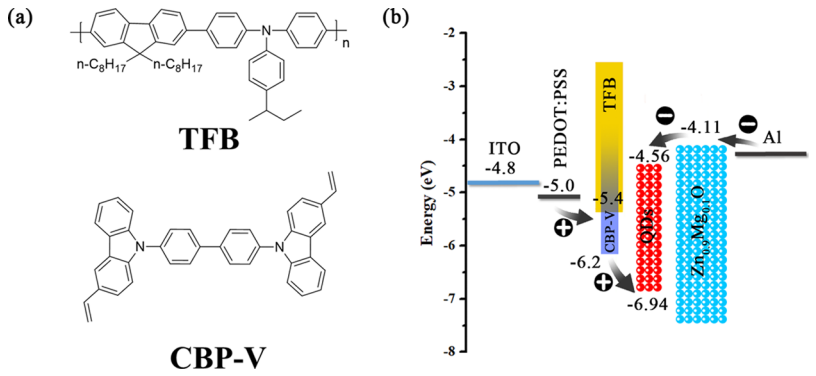

Figure 1. (a) Chemical structures of the polymer HTM TFB and cross-linkable small-molecule HTM CBP-V. (b) Schematic of the device structure, the energy level of the materials, and holes transporting from the hole injection layer (HIL) to QD layer.

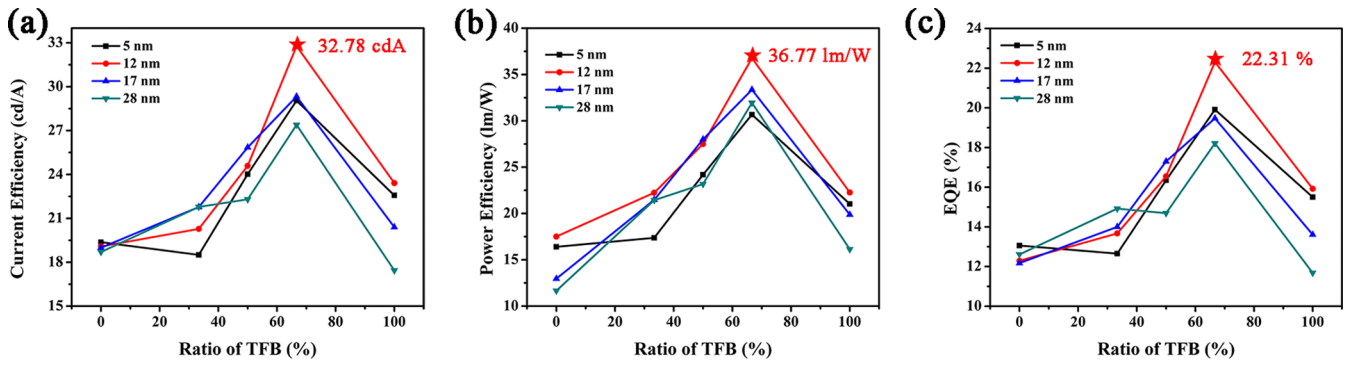

Figure 2. Maximum (a) CE, (b) PE, and (c) EQE of red QLEDs with different HTLs at different thicknesses.

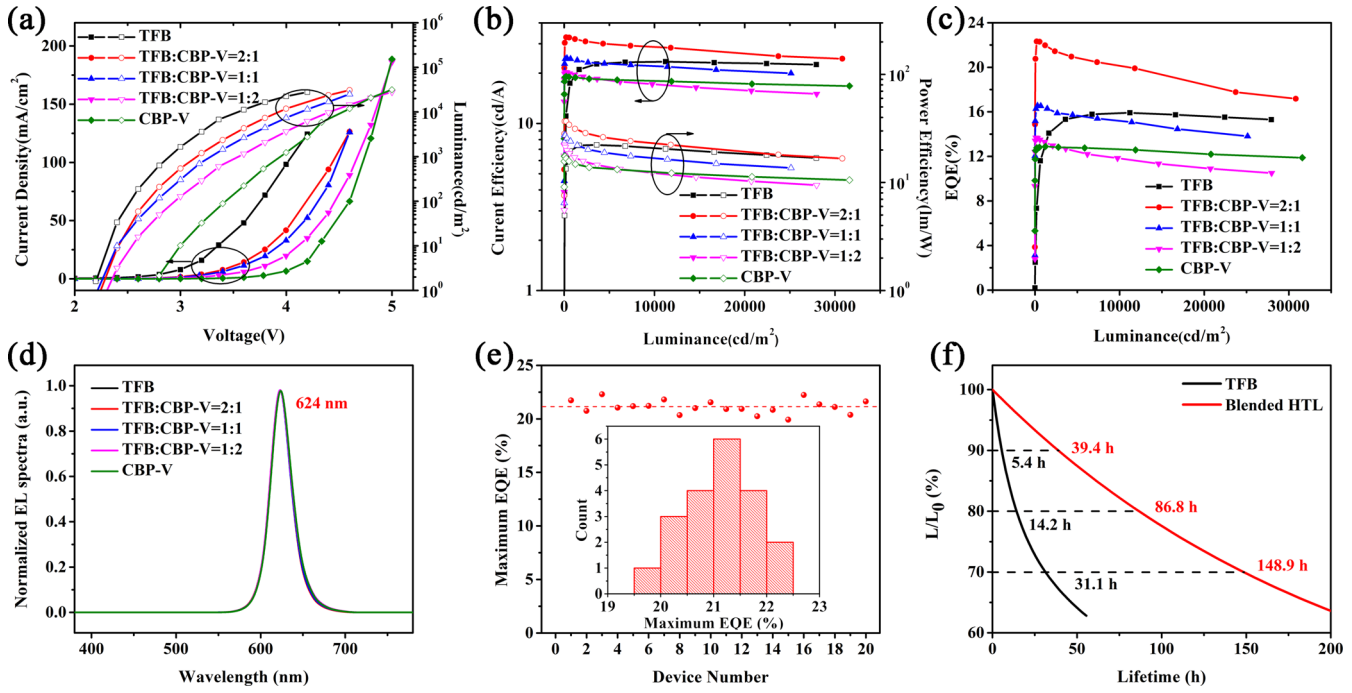

Figure 3. At the optimal HTL thickness of 12 nm, (a) *J*−*V*−*L*, (b) CE−*L*−PE, (c) EQE−*L* characteristics, and (d) normalized EL spectra of the devices with different HTLs. (e) Histogram of maximum EQE of the optimal blended HTL devices measured from 20 devices. (f) Lifetime of the TFB-only device and optimal blended HTL device.

printable using an inkjet printer, and higher boiling point solvents should be used to avoid inkjet nozzle blocking. The inkjet printing technology has been applied to prepare interfacial functional layers in optoelectronic devices.[32−35] The cross-linking process[2,36−45] can well solve the problem. The authors' group recently reported a novel cross-linkable small molecular HTM 4,4′-bis(3-vinyl-9*H*-carbazol-9-yl)1,1′-biphenyl (CBP-V) for inkjet-printed QLEDs.[46] CBP-V has a

https://dx.doi.org/10.1021/acsami.0c01001
ACS Appl. Mater. Interfaces 2020, 12, 13087−13095

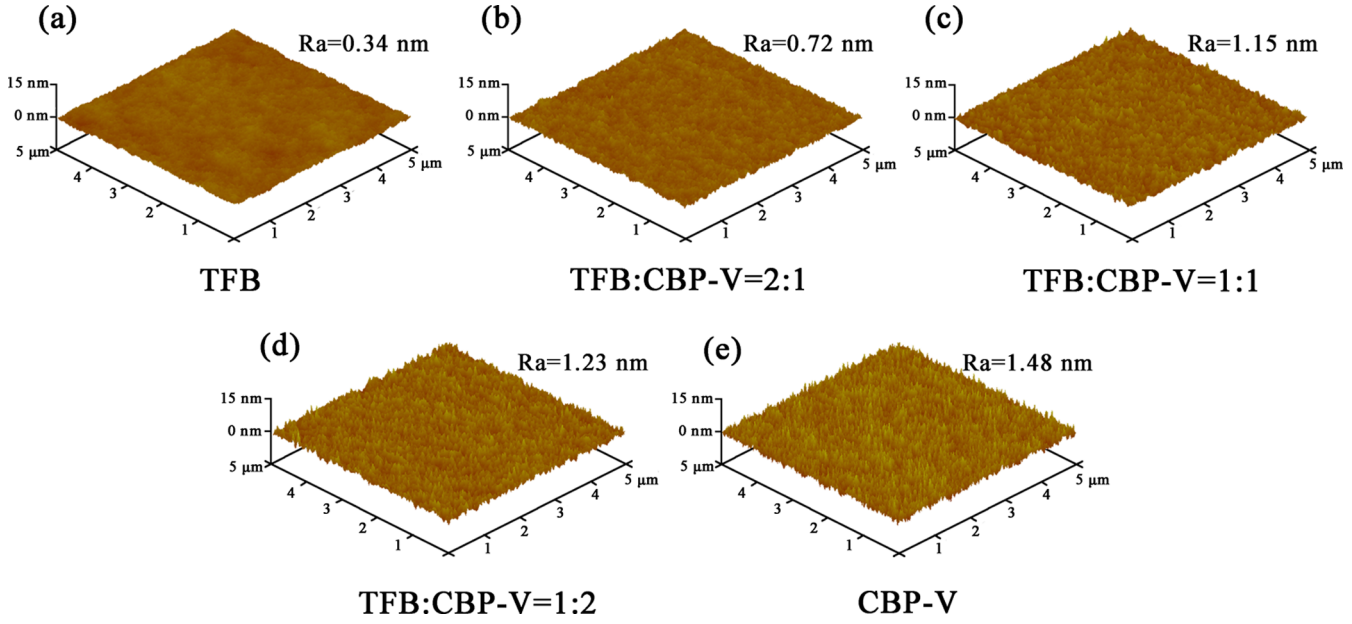

Figure 4. AFM images: (a) TFB, (b) TFB/CBP-V = 2:1, (c) TFB/CBP-V = 1:1, (d) TFB/CBP-V = 1:2, and (e) CBP-V.

deep HOMO level of −6.2 eV, good solvent resistance, and very high thermal stability after cross-linking, provided a stable interface of HTL/QDs. Though the hole injection is much improved at CBP-V/QDs interface, the driving voltage is still high.

In this work, a new HTL blending polymer TFB (HOMO ∼−5.4 eV) and cross-linkable small molecule CBP-V (HOMO ∼−6.2 eV) are presented for red QLEDs. They have been proved to play a crucial role in decreasing the hole-injection barrier from indium tin oxide (ITO) to the HTL and then from the HTL to QD emitting layer. The carrier transport is more balanced and the exciton recombination is enhanced. Compared with the TFB-only devices, red QLEDs with the blended HTL had the EQE enhanced from 15.9 to 22.3% without increasing the turn-on voltage for the spin-coating-fabricated device. Furthermore, the blended HTL prolonged the T_{90} and T_{70} lifetime from 5.4 and 31.1 to 39.4 and 148.9 h, respectively. These enhancements in lifetime are attributed to the low hole-injection barrier at the HTL/QD interface and high thermal stability of the blended HTL after cross-linking. Moreover, the blended HTL showed excellent solvent resistance after cross-linking. Based on this, the inkjet-printed red QLEDs were fabricated. The EQE of the inkjet-printed red QLEDs reached 16.89%.

RESULTS AND DISCUSSION

Optimization of the TFB and CBP-V Ratio. The chemical structures of the polymer HTM TFB and cross-linkable small-molecule HTM CBP-V are shown in Figure 1a. To optimize the weight ratio of TFB and CBP-V for the blending and the thickness of the blended HTL, red QLED devices with the layer structure ITO (160 nm)/PEDOT:PSS (35 nm)/HTL (5, 12, 17 or 28 nm)/QDs (20 nm)/$Zn_{0.9}Mg_{0.1}O$ (50 nm)/Al (100 nm) were fabricated by spin-coating. The schematic of the device structure and the energy level of the materials are shown in Figure 1b. Three weight ratios of TFB and CBP-V of 2:1, 1:1, and 1:2 were investigated. The maximum current efficiency (CE), power efficiency (PE), and EQE for these blended HTLs at different thickness are shown in Figure 2. When the weight ratio was 2:1, the devices showed the best performance for all the four different thicknesses, and the highest EQE of 22.3% was achieved when the thickness was 12 nm.

Figure 3 shows the $J-V-L$, CE−L−PE, and EQE−L characteristics of QLEDs with different weight ratios of blended HTLs at the optimal thickness of 12 nm. The data for other thicknesses are shown in Figure S1 in the Supporting Information. Their performances are summarized in Table S1. Figure 3d shows the normalized electroluminescence (EL) spectra. EL spectra of the QLEDs were not affected by the different HTLs. Owing to the lower HOMO energy level of TFB, the TFB-only device had a low turn-on voltage of 2.2 V, compared with the CBP-V-only device. When the content of TFB increased from 0 to 33%, the turn-on voltage declined from 2.7 to 2.3 V with the HTL thickness of 12 nm. When the weight ratio of TFB and CBP-V was 1:1 and 2:1, the turn-on voltage was 2.2 V, which is almost the same as that of the TFB-only device. When the thickness of HTLs increased from 12 to 28 nm, the turn-on voltages of the blended HTL increased by less than 0.05 V, whereas the turn-on voltage of TFB-only devices increased about 0.2 V and the turn-on voltage of CBP-V-only devices increased over 0.8 V.

TFB has the shallower HOMO energy level, and CBP-V has the deeper HOMO. The introduction of CBP-V reduces the injection barrier from the HTL to QD layer, compared with the TFB-only device. Combining these two HTMs to form the blended HTL can reduce the injection barrier from the HIL to QD layer so as to reduce the turn-on voltage. On the other hand, as the ratio of TFB increases, the current density increases. The presence of TFB in the blended HTL guarantees high mobility, compared with the CBP-V-only device. The optimal weight ratio of TFB and CBP-V was found to be 2:1. At this ratio, the blended HTL created a balance between the injection barrier from the HTL to QD layer and hole mobility. As shown in Figure 1b, holes would mostly inject from CBP-V to QDs rather than from TFB to QDs at the HTL/QD interface because of the lower hole injection barrier. Thus, the hole injection from the HTL to QD layer is

https://dx.doi.org/10.1021/acsami.0c01001
ACS Appl. Mater. Interfaces 2020, 12, 13087−13095

improved to reach the balance between holes and electrons. Also, better balance between the injection barrier and hole mobility made the devices less sensitive to the thickness of the HTL, as mentioned above.

Compared with the TFB-only HTL, the blended HTL enhanced the CE, PE, and EQE from 23.4 cd/A, 22.3 lm/W, and 15.9% to 32.8 cd/A, 36.8 lm/W, and 22.3%, respectively. The average maximum EQE measured from 20 devices was 21.1% with the distribution from 19.9 to 22.3%, as the histogram of the maximum EQE is shown in Figure 3e, which indicated the high reproducibility of the blended HTL devices. The operational lifetimes of devices with the TFB HTL and blended HTL were investigated at an initial luminance of ~2000 cd/m^2. The T_{90}, T_{80}, and T_{70} lifetimes were prolonged from 5.4, 14.2, and 31.1 to 39.4, 86.8, and 148.9 h, respectively, which was attributed to the stable interface of HTL/QDs with low oxidation potential and high thermal stability.

Mechanism of the Blended HTL. The improvement mechanism of the blended HTL was investigated. The film morphologies of various HTLs were inspected by atomic force microscopy (AFM). All the HTLs (12 nm) were spin-coated on the substrates of ITO/PEDOT:PSS. All the films showed low roughness with the average roughness less than 2 nm. As shown in Figure 4, the TFB-only HTL has the lowest roughness, and the roughness of the blended HTL is between that of TFB and CBP-V HTLs. The roughness of blended HTLs is lower when the ratio of TFB is higher. As AFM phase graphs show (Figure S2), TFB and CBP-V were blended uniformly without phase separation in all the ratios others reported.[24,26] Low roughness and no phase separation at the blending ratio of 2:1 resulted in better photoelectric performance.

To investigate the charge transfer from the QD layer to HTL, the time-resolved photoluminescence (TRPL) of QDs on different substrates were measured. The structures of the samples were glass/QDs, glass/TFB/QDs, glass/CBP-V/QDs, and glass/blended HTL/QDs. The TRPL spectra of QD-only film and QD film on different HTLs are shown in Figure 5,

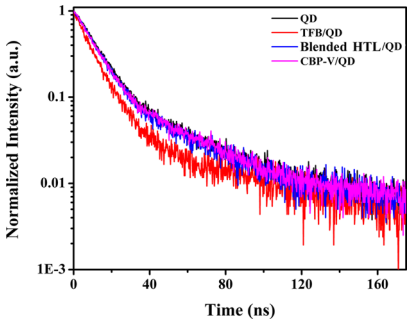

Figure 5. TRPL of the QD-only film and QD films on different HTLs.

where the TRPL curves were fitted using a bi-exponential equation. The average photoluminescence lifetimes (τ_{ave}) of the QD-only film and QD films on TFB, blended HTL, and CBP-V were 34.27, 26.45, 30.91, and 32.35 ns, respectively. The τ_{ave} of the QD film on TFB was the shortest, which is related with the spontaneous charge transfer from the QD layer to HTL.[7] The CBP-V in the blended HTL helps suppress exciton quenching, which improves the device performance.

Electrochemical impedance spectroscopy (EIS), which has been widely applied for characterizing photovoltaic devices,[47,48] was also applied to investigate the physical processes in light-emitting diode devices.[49−52] To further investigate the improvement mechanism of blended HTL devices, EIS spectra were measured with a frequency range from 1 Hz to 1 MHz, and the forward bias was 3 V. Figure 6 shows the measured

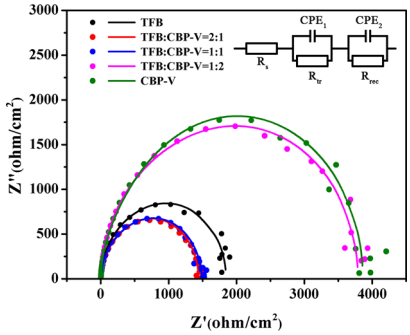

Figure 6. Measured Nyquist plots of EIS spectra of red QLEDs with different HTLs and their fitting curves. The simplified equivalent circuit of the devices is shown in the inset.

Nyquist plots of EIS spectra of QLEDs with different HTLs and their fitting curves. The simplified equivalent circuit is shown in the inset of Figure 6, composed of a series resistance (R_s) and two R//CPE (constant phase element) parallels. The series resistance is the overall external resistance including the electrodes, external wires, and the contact resistance between the electrodes and the functional layers.[53] The first R//CPE composited of R_{tr} and CPE_1 is related to the charge transport process. R_{tr} is the charge-transfer-related resistance and CPE_1 is the interface capacitance of charge transport layers.[54] The second R//CPE composited of R_{rec} and CPE_2 is related to the recombination process. R_{rec} is the recombination resistance which is defined as the reverse derivative of voltage as a function of the recombination current.[51] CPE_2 is the chemical capacitance of the recombination area.[51] The fitting parameters for various devices with different HTLs are shown in Table S3. R_{tr} can be seen as the sum of hole transport resistance and electron transport resistance.[55] All the devices have the same electron transport layer, so R_{tr} can reflect the hole mobility of different HTLs.

The TFB-only device has the smallest R_{tr}, while that of the CBP-V only device is the largest. With the ratio of TFB in the blended HTL increased, R_{tr} reduced. This trend agrees well with the $J-V$ curves of these devices. The smaller R_{rec} indicates the higher recombination rate. The CBP-V-only device has the highest R_{rec} at 3 V because of its higher turn-on voltage of 2.7 V. The luminance of the CBP-V device is one to 2 orders of magnitude lower than that of the other devices. For the other four devices, the TFB device has the highest luminance, but its R_{rec} is the largest, which means its recombination rate is the lowest. The presence of CBP-V in blended HTLs improved the recombination rate. Although TFB had higher hole mobility to provide higher current density, the hole current could not recombine effectively with the electron current. Compared with the TFB HTL, the blended HTL reduced its hole mobility in exchange for a higher recombination rate to achieve higher device performance.

The hole-only devices (HODs) of different HTLs with the structure of ITO (160 nm)/PEDOT (35 nm)/HTL (12 nm)/QDs (20 nm)/MoO_3 (5 nm)/Al (100 nm) were fabricated to investigate the hole transport ability of TFB, CBP-V, and

https://dx.doi.org/10.1021/acsami.0c01001
ACS Appl. Mater. Interfaces 2020, 12, 13087−13095

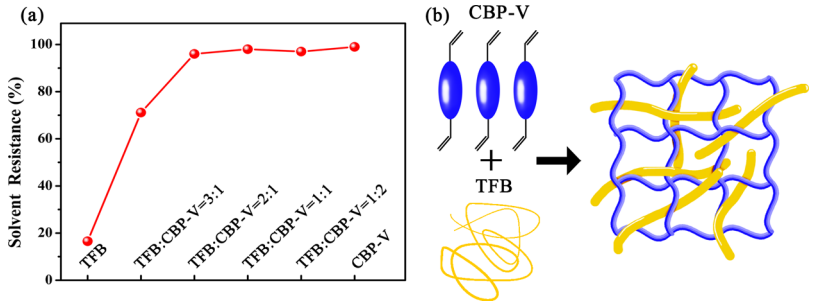

Figure 7. (a) Solvent resistance of different HTLs. (b) Schematic of the cross-linking process of the blended HTL.

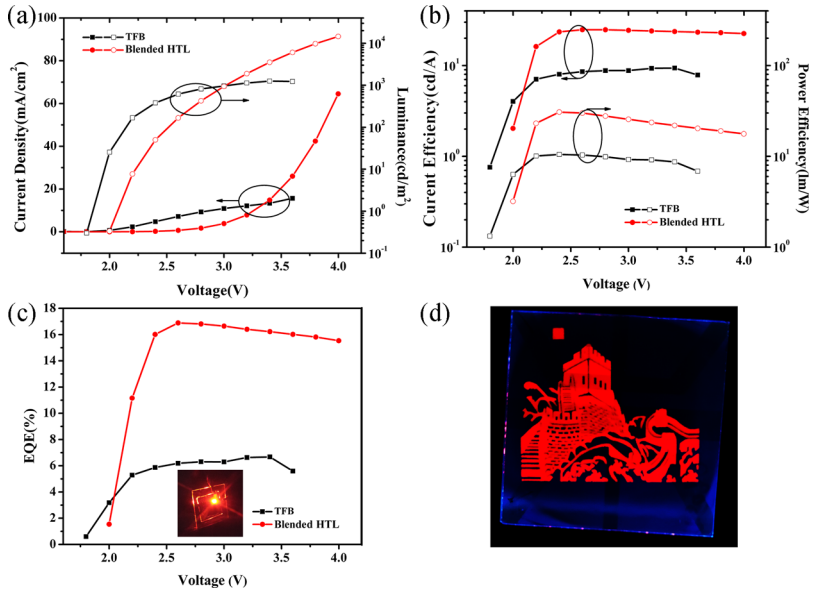

Figure 8. (a) *J*−*V*−*L*, (b) CE−*L*−PE, and (c) EQE−*L* characteristics of the inkjet-printed QLEDs with TFB and blended HTL. (d) Photoluminescence photograph of the Great Wall pattern printed on the blended HTL. Inset of (c) is the EL image of the inkjet-printed blended HTL device.

blended HTL. As shown in Figure S3, the TFB device has higher hole current density than the CBP-V device, and the introduction of CBP-V decreased the hole current density, which indicates the lower hole mobility of the blended HTL and CBP-V. The turning point of the *J*−*V* curve for the blended HTL device, which reflects the threshold voltage from the Ohmic conduction type to the space charge-limited conduction type,[56] declines from 2.8 to 0.9 V, compared with the CBP-V device. The TFB in blended HTL devices helps achieve higher hole mobility and lower injection barrier at the HIL/HTL interface than CBP-V devices. This result is consistent with the analysis of impedance spectra discussed above.

Solvent Resistance of the Blended HTLs. The solvent resistant property of the CBP-V, TFB, and blended HTLs was investigated using UV−vis spectroscopy. Chlorobenzene, which was the main solvent in the QD ink of this work, was tested for the resistance of blended HTL films with a weight ratio of TFB and CBP-V of 3:1, 2:1, 1:1, and 1:2. All the films were cured at 200 °C for 60 min. The UV−vis absorption spectra of the cured films of different HTLs before and after rinsing with chlorobenzene are shown in Figure S4. The solvent resistances (decline of UV−vis spectral intensity after rinsing with chlorobenzene) of different HTLs are shown in Figure 7a. The UV−vis spectral intensity of TFB declines seriously after rinsing with chlorobenzene, which indicates the poor solvent resistance of the TFB film. When the weight ratio of TFB and CBP-V is 3:1, the blended HTL has partial solvent resistance. When the weight ratio of TFB and CBP-V is ≤2:1, the films showed excellent solvent resistance. If the content of CBP-V reaches a certain proportion, CBP-V could form an integral insoluble mesh, and the TFB polymer was embedded in the mesh (Figure 7b) without being dissolved by the solvents. Therefore, the whole layer shows excellent solvent resistance. As shown in Figure S5, the blended HTL demonstrated solvent resistance to other solvents as well, such as toluene, phenylcyclohexane, and so forth. The good thermal stability of the cross-linked HTL makes the interface of HTL/QDs more stable, which improves the device performance, especially the device lifetime.

Inkjet-Printed QLEDs. Red QLED devices were fabricated by inkjet-printing QD ink on TFB and blended HTLs. The concentration of the red QD ink was 12 mg/mL. The solvents used in the red QD ink were chlorobenzene and tetradecane, and their volume ratio was 9:1. The surface energy of different HTLs was calculated by measuring the contact angles of deionized water and diiodomethane on the corresponding HTLs. Figure S6 shows the results, and Table S4 shows the surface energy of different HTLs. CBP-V had the highest surface energy of 42.19 mN/m and that of TFB was 34.17

https://dx.doi.org/10.1021/acsami.0c01001
ACS Appl. Mater. Interfaces 2020, 12, 13087−13095

mN/m. When the weight ratio of TFB and CBP-V in the blended HTL was ≤1:1, its surface energy was lower than that of TFB. The surface energy at the weight ratio of 2:1 was 35.44 mN/m, which was more suitable for inkjet printing than the other two blended HTLs. It is not clear yet why the surface energy of the other two blended HTLs was even lower than that of TFB, which needs to be further investigated. Figure S7 shows the graphs of ink spreading on different blended HTLs. The QD ink could not spread well on the blended HTLs with the TFB/CBP-V ratio of 1:2 and 1:1 but spread well for the TFB/CBP-V ratio of 2:1 and form uniform lines and squares because of its higher surface energy. Figure 8d shows the photoluminescence photograph of a pattern printed on the blended HTL. Figure 8a–c shows the J–V–L, CE–L–PE, and EQE–L characteristics of inkjet-printed QLEDs with TFB and blended HTLs, and the performances of the TFB devices and blended HTL devices using both spin-coating and inkjet-printing are summarized in Table 1. The inkjet-printed TFB device has higher current density but poorer performance because of its poor solvent resistance. In the inkjet-printing process, the chlorobenzene in the QD ink dissolved the TFB and destroyed the film. For the blended HTL devices, the main HTM at the interface of HTL/QD was CBP-V because parts of TFB coated on the surface were removed by the solvent of the QD ink, which further enhanced hole injection to the QD layer. The turn-on voltage of the inkjet-printed device was slightly lower than that of the spin-coated device because of the thinner thickness of the inkjet-printed QD layer (~17 nm). The EQE of inkjet-printed QLEDs with the blended HTL reached 16.9%, which is attributed to the excellent solvent resistance and the improvement to device performance of the blended HTL. The PE reached 30.7 lm/W, which is the highest for inkjet-printed red QLEDs reported so far, because of the low operating voltage (Figure 9).

Table 1. Summarized Performance of Spin-Coated and Inkjet-Printed QLEDs with Different HTLs at Different Thickness

HTL type	preparation for QDs layer	V_T (V)[a]	CE_{Max} (cd/A)	PE_{Max} (lm/W)	EQE_{Max} (%)
blended HTL	spin coating	2.2	32.8	36.8	22.3
	inkjet printing	2.1	24.8	30.7	16.9
TFB	spin coating	2.2	23.4	22.3	15.9
	inkjet printing	1.8	9.4	10.5	6.7

[a] V_T: turn-on voltage, defined as the voltage when the luminance reaches 1 cd/m^2.

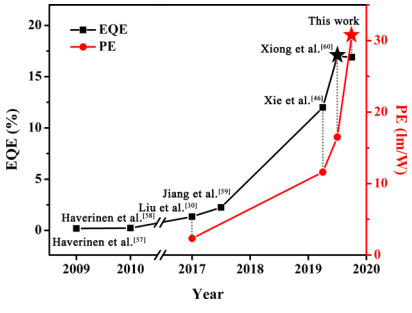

Figure 9. Evolution of the reported EQE and power efficiency of inkjet-printed red QLEDs.[57−60]

CONCLUSIONS

Cross-linkable small molecular CBP-V and polymer TFB have been blended to create a new HTM. The introduction of CBP-V has reduced the injection barrier from the HTL to QD layer, enhanced the hole transport from the HIL to QD layer, and improved the recombination efficiency to achieve better balance between hole current and electron current. The existence of CBP-V in the blend makes the interface of HTL/QDs more stable because of the good thermal stability of the film after cross-linking. Exciton quenching has also been suppressed with the existence of CBP-V. For spin-coated red QLEDs, the CE, PE, and EQE have been enhanced from 23.41 cd/A, 22.27 lm/W, and 15.92% for devices with the TFB-only HTL to 32.78 cd/A, 36.77 lm/W, and 22.31% for devices with the blended HTL at the TFB to CBP-V ratio of 2:1. The T_{90} lifetime at ~2000 cd/m^2 has been prolonged from 5.4 to 39.4 h. In addition, the blended HTL showed excellent solvent resistance after cross-linking. Red QLEDs have also been fabricated by the inkjet printing method and have an EQE of 16.9%. The PE reached 30.73 lm/W, which is the highest reported so far for inkjet-printed red QLEDs. The blended HTL also improved the performance of the blue and green cadmium-based QLEDs, which will be reported elsewhere. The new solvent-resistant blended HTL paves the way for further development of highly efficient and stable printed QLEDs.

EXPERIMENTAL SECTION

Synthesis of $Zn_{0.9}Mg_{0.1}O$ NPs. The synthesis method of $Zn_{0.9}Mg_{0.1}O$ NPs was based on the work of Xie.[46]

Fabrication of QLED Devices. Before fabricating QLED devices, the ITO glass substrates were scrubbed with solvents and treated with oxygen plasma for 3 min. PEDOT:PSS (Heraeus Clevios, AI 4083) was spin-coated on ITO glasses as the HIL at 4000 rpm for 35 s. Then, the samples were dried at 130 °C for 15 min to remove the residual solvent in a nitrogen-filled glovebox (O_2 < 1 ppm, H_2O < 1 ppm). TFB (Xi'an Polymer Light Technology Corp.) and CBP-V were dissolved in chlorobenzene and mixed with different weight ratios. The TFB, CBP-V, and blended HTMs were spin-coated at 3000 rpm for 30 s. Then, all the samples were annealed at 130 °C for 10 min to remove the residual solvent, followed by curing at 200 °C for 60 min for cross-linking. For the spin-coating devices, the red CdZnSe/ZnS QDs (Jiaxing Nato Optoelectronic Technology Corp.) in octane were spin-coated at 3000 rpm for 30 s. For the inkjet-printed devices, the QDs were dispersed in the mixed solvent of chlorobenzene and tetradecane with the volume ratio of 9:1.[46] The QD ink was inkjet-printed on the substrates using a DMP-2831 inkjet printer (Fujifilm Co.). Then, the $Zn_{0.9}Mg_{0.1}O$ NPs were spin-coated at 3000 rpm for 30 s and annealed at 90 °C for 15 min. The Al cathode was deposited in a vacuum of 2 × 10^{-4} Pa with vacuum deposition. Finally, the devices were encapsulated with glass and ultraviolet-curable epoxy.

Characterizations and Device Measurement. The electroluminescence spectrum was measured with a Spectra Scan PR655. The current–voltage (I–V) and luminance–voltage (L–V) relations were characterized with a computer-controlled Keithley 2400 sourcemeter. The thicknesses of the films were measured using an Alpha Step profilometer (Veeco, Dektak150). The active area of all the devices was 2 × 2 mm^2. The film surface morphology was characterized using a Veeco Dimension 3100 in the tapping mode. The fluorescence decay was characterized using an Edinburgh FLS920 phosphorescence lifetime system equipped with a 375 nm laser at room temperature. EIS was performed with a PGSTAT302N electrochemical workstation. UV–vis absorption spectra were characterized using a PerkinElmer Lambda 750. The contact angle data were measured using an optical contact angle and interface tension meter (SL150L).

https://dx.doi.org/10.1021/acsami.0c01001
ACS Appl. Mater. Interfaces 2020, 12, 13087−13095

■ ASSOCIATED CONTENT

Supporting Information

The Supporting Information is available free of charge at https://pubs.acs.org/doi/10.1021/acsami.0c01001.

Summarized performances of the red QLEDs with different HTLs at different thicknesses; AFM phase graphs of different HTLs; fitting parameters for the TRPL spectra; fitting parameters of the Nyquist plots for QLEDs at 3 V; $J-V$ characteristics of the HODs with different HTLs; UV−vis absorption spectra of the cured films of different HTLs before and after rinsing with chlorobenzene; contact angles and the calculated surface energy of different HTLs; and photographs of inkjet printing on different HTLs (PDF)

■ AUTHOR INFORMATION

Corresponding Authors

Jinyong Zhuang − *Guangdong Juhua Printed Display Technol Company Ltd, Guangzhou, Guangdong 510700, People's Republic of China*; Email: zhuangjinyong@tcl.com

Wenming Su − *Printable Electronics Research Center, Suzhou Institute of Nano-Tech and Nano-Bionics, Chinese Academy of Sciences, Suzhou, Jiangsu 215123, People's Republic of China; School of Nano-Tech and Nano-Bionics, University of Science and Technology of China, Hefei, Anhui 230026, People's Republic of China*; orcid.org/0000-0003-1721-1923; Email: wmsu2008@sinano.ac.cn

Authors

Pengyu Tang − *Printable Electronics Research Center, Suzhou Institute of Nano-Tech and Nano-Bionics, Chinese Academy of Sciences, Suzhou, Jiangsu 215123, People's Republic of China; School of Nano-Tech and Nano-Bionics, University of Science and Technology of China, Hefei, Anhui 230026, People's Republic of China*

Liming Xie − *Printable Electronics Research Center, Suzhou Institute of Nano-Tech and Nano-Bionics, Chinese Academy of Sciences, Suzhou, Jiangsu 215123, People's Republic of China*

Xueying Xiong − *Printable Electronics Research Center, Suzhou Institute of Nano-Tech and Nano-Bionics, Chinese Academy of Sciences, Suzhou, Jiangsu 215123, People's Republic of China; School of Nano-Tech and Nano-Bionics, University of Science and Technology of China, Hefei, Anhui 230026, People's Republic of China*

Changting Wei − *Printable Electronics Research Center, Suzhou Institute of Nano-Tech and Nano-Bionics, Chinese Academy of Sciences, Suzhou, Jiangsu 215123, People's Republic of China*; orcid.org/0000-0003-2512-4643

Wenchao Zhao − *Printable Electronics Research Center, Suzhou Institute of Nano-Tech and Nano-Bionics, Chinese Academy of Sciences, Suzhou, Jiangsu 215123, People's Republic of China*

Ming Chen − *Printable Electronics Research Center, Suzhou Institute of Nano-Tech and Nano-Bionics, Chinese Academy of Sciences, Suzhou, Jiangsu 215123, People's Republic of China*

Zheng Cui − *Printable Electronics Research Center, Suzhou Institute of Nano-Tech and Nano-Bionics, Chinese Academy of Sciences, Suzhou, Jiangsu 215123, People's Republic of China; School of Nano-Tech and Nano-Bionics, University of Science and Technology of China, Hefei, Anhui 230026, People's Republic of China*

Complete contact information is available at: https://pubs.acs.org/10.1021/acsami.0c01001

Author Contributions

‖P.T. and L.X. contributed equally.

Notes

The authors declare no competing financial interest.

■ ACKNOWLEDGMENTS

This work was financially supported by the National Natural Science Foundation of China (U1605244), National Key Research and Development Program of China (2016YFB0401600), Youth Innovation Promotion Association CAS (no. 2013206), and the State Key Laboratory of Advanced Technologies for Comprehensive Utilization of Platinum Metals (SKL-SPM-201807). The authors also appreciate Guangdong Juhua Printed Display Technology Co., Ltd. for financial support.

■ REFERENCES

(1) Alivisatos, A. P. Semiconductor Clusters, Nanocrystals, and Quantum Dots. *Science* **1996**, *271*, 933−937.

(2) Niu, Y. H.; Munro, A. M.; Cheng, Y.-J.; Tian, Y. Q.; Liu, M. S.; Zhao, J. L.; Bardecker, J. A.; Jen-La Plante, I.; Ginger, D. S.; Jen, A. K.-Y. Improved Performance from Multilayer Quantum Dot Light-Emitting Diodes via Thermal Annealing of the Quantum Dot Layer. *Adv. Mater.* **2007**, *19*, 3371−3376.

(3) Sun, Q.; Wang, Y. A.; Li, L. S.; Wang, D.; Zhu, T.; Xu, J.; Yang, C.; Li, Y. Bright, Multicoloured Light-Emitting Diodes Based on Quantum Dots. *Nat. Photonics* **2007**, *1*, 717−722.

(4) Bae, W. K.; Kwak, J.; Lim, J.; Lee, D.; Nam, M. K.; Char, K.; Lee, C.; Lee, S. Multicolored Light-Emitting Diodes Based on All-Quantum-Dot Multilayer Films Using Layer-by-Layer Assembly Method. *Nano Lett.* **2010**, *10*, 2368−2373.

(5) Qian, L.; Zheng, Y.; Xue, J.; Holloway, P. H. Stable and Efficient Quantum-Dot Light-Emitting Diodes Based on Solution-Processed Multilayer Structures. *Nat. Photonics* **2011**, *5*, 543−548.

(6) Lee, K.-H.; Lee, J.-H.; Song, W.-S.; Ko, H.; Lee, C.; Lee, J.-H.; Yang, H.; Yang, H. Highly Efficient, Color-Pure, Color-Stable Blue Quantum Dot Light-Emitting Devices. *ACS Nano* **2013**, *7*, 7295−7302.

(7) Dai, X.; Zhang, Z.; Jin, Y.; Niu, Y.; Cao, H.; Liang, X.; Chen, L.; Wang, J.; Peng, X. Solution-Processed, High-Performance Light-Emitting Diodes Based on Quantum Dots. *Nature* **2014**, *515*, 96−99.

(8) Bae, W. K.; Lim, J.; Lee, D.; Park, M.; Lee, H.; Kwak, J.; Char, K.; Lee, C.; Lee, S. R/G/B/Natural White Light Thin Colloidal Quantum Dot-Based Light-Emitting Devices. *Adv. Mater.* **2014**, *26*, 6387−6393.

(9) Song, J.; Li, J.; Li, X.; Xu, L.; Dong, Y.; Zeng, H. Quantum Dot Light-Emitting Diodes Based on Inorganic Perovskite Cesium Lead Halides (CsPbX3). *Adv. Mater.* **2015**, *27*, 7162−7167.

(10) Li, X.; Wu, Y.; Zhang, S.; Cai, B.; Gu, Y.; Song, J.; Zeng, H. CsPbX3Quantum Dots for Lighting and Displays: Room-Temperature Synthesis, Photoluminescence Superiorities, Underlying Origins and White Light-Emitting Diodes. *Adv. Funct. Mater.* **2016**, *26*, 2435−2445.

(11) Kim, B. H.; Nam, S.; Oh, N.; Cho, S.-Y.; Yu, K. J.; Lee, C. H.; Zhang, J.; Deshpande, K.; Trefonas, P.; Kim, J.-H.; Lee, J.; Shin, J. H.; Yu, Y.; Lim, J. B.; Won, S. M.; Cho, Y. K.; Kim, N. H.; Seo, K. J.; Lee, H.; Kim, T.-i.; Shim, M.; Rogers, J. A. Multilayer Transfer Printing for Pixelated, Multicolor Quantum Dot Light-Emitting Diodes. *ACS Nano* **2016**, *10*, 4920−4925.

(12) Li, J.; Xu, L.; Wang, T.; Song, J.; Chen, J.; Xue, J.; Dong, Y.; Cai, B.; Shan, Q.; Han, B.; Zeng, H. 50-Fold EQE Improvement up to 6.27% of Solution-Processed All-Inorganic Perovskite CsPbBr3 QLEDs via Surface Ligand Density Control. *Adv. Mater.* **2017**, *29*, 1603885.

(13) Dai, X.; Deng, Y.; Peng, X.; Jin, Y. Quantum-Dot Light-Emitting Diodes for Large-Area Displays: Towards the Dawn of Commercialization. *Adv. Mater.* **2017**, *29*, 1607022.

(14) Chang, J. H.; Park, P.; Jung, H.; Jeong, B. G.; Hahm, D.; Nagamine, G.; Ko, J.; Cho, J.; Padilha, L. A.; Lee, D. C.; Lee, C.; Char, K.; Bae, W. K. Unraveling the Origin of Operational Instability of Quantum Dot Based Light-Emitting Diodes. *ACS Nano* **2018**, *12*, 10231−10239.
(15) Yang, D.; Li, X.; Zhou, W.; Zhang, S.; Meng, C.; Wu, Y.; Wang, Y.; Zeng, H. CsPbBr 3 Quantum Dots 2.0: Benzenesulfonic Acid Equivalent Ligand Awakens Complete Purification. *Adv. Mater.* **2019**, *31*, 1900767.
(16) Li, X.; Lin, Q.; Song, J.; Shen, H.; Zhang, H.; Li, L. S.; Li, X.; Du, Z. Quantum-Dot Light-Emitting Diodes for Outdoor Displays with High Stability at High Brightness. *Adv. Opt. Mater.* **2020**, *8*, 1901145.
(17) Zhang, H.; Hu, N.; Zeng, Z.; Lin, Q.; Zhang, F.; Tang, A.; Jia, Y.; Li, L. S.; Shen, H.; Teng, F.; Du, Z. High-Efficiency Green InP Quantum Dot-Based Electroluminescent Device Comprising Thick-Shell Quantum Dots. *Adv. Opt. Mater.* **2019**, *7*, 1801602.
(18) Redecker, M.; Bradley, D. D. C.; Inbasekaran, M.; Wu, W. W.; Woo, E. P. High Mobility Hole Transport Fluorene-Triarylamine Copolymers. *Adv. Mater.* **1999**, *11*, 241−246.
(19) Chen, S.; Cao, W.; Liu, T.; Tsang, S. W.; Yang, Y.; Yan, X.; Qian, L. On the Degradation Mechanisms of Quantum-Dot Light-Emitting Diodes. *Nat. Commun.* **2019**, *10*, 765.
(20) Shen, H.; Gao, Q.; Zhang, Y.; Lin, Y.; Lin, Q.; Li, Z.; Chen, L.; Zeng, Z.; Li, X.; Jia, Y.; Wang, S.; Du, Z.; Li, L. S.; Zhang, Z. Visible Quantum Dot Light-Emitting Diodes with Simultaneous High Brightness and Efficiency. *Nat. Photonics* **2019**, *13*, 192−197.
(21) Song, J.; Wang, O.; Shen, H.; Lin, Q.; Li, Z.; Wang, L.; Zhang, X.; Li, L. S. Over 30% External Quantum Efficiency Light-Emitting Diodes by Engineering Quantum Dot-Assisted Energy Level Match for Hole Transport Layer. *Adv. Funct. Mater.* **2019**, *29*, 1808377.
(22) Yu, J. C.; Jang, J. I.; Lee, B. R.; Lee, G.-W.; Han, J. T.; Song, M. H. Highly Efficient Polymer-Based Optoelectronic Devices Using PEDOT:PSS and a GO Composite Layer as a Hole Transport Layer. *ACS Appl. Mater. Interfaces* **2014**, *6*, 2067−2073.
(23) Li, J.; Liang, Z.; Su, Q.; Jin, H.; Wang, K.; Xu, G.; Xu, X. Small Molecule Modified Hole Transport Layer Targeting Low Turn-on Voltage, Bright and Efficient Full-color Quantum Dot Light Emitting Diodes. *ACS Appl. Mater. Interfaces* **2018**, *10*, 3865−3873.
(24) Lee, J.; Kim, G.; Shin, D.-K.; Seo, Y.; Kim, K.; Park, J. Improved Surface Morphology of Crosslinked Hole Transport Films by a Mixture of Polymer for OLEDs. *IEEE Trans. Electron Devices* **2018**, *65*, 3311−3317.
(25) Zhang, Z.; Ye, Y.; Pu, C.; Deng, Y.; Dai, X.; Chen, X.; Chen, D.; Zheng, X.; Gao, Y.; Fang, W.; Peng, X.; Jin, Y. High-Performance, Solution-Processed, and Insulating-Layer-Free Light-Emitting Diodes Based on Colloidal Quantum Dots. *Adv. Mater.* **2018**, *30*, 1801387.
(26) Park, S.-R.; Kang, J.-H.; Ahn, D. A.; Suh, M. C. A Cross-Linkable Hole Transport Material Having Improved Mobility Through a Semi-Interpenetrating Polymer Network Approach for Solution-Processed Green PHOLEDs. *J. Mater. Chem. C* **2018**, *6*, 7750−7758.
(27) Tsai, K.-W.; Hung, M.-K.; Mao, Y.-H.; Chen, S.-A. Solution-Processed Thermally Activated Delayed Fluorescent OLED with High EQE as 31% Using High Triplet Energy Crosslinkable Hole Transport Materials. *Adv. Funct. Mater.* **2019**, *29*, 1901025.
(28) Zhang, Y.; Huang, F.; Chi, Y.; Jen, A. K.-Y. Highly Efficient White Polymer Light-Emitting Diodes Based on Nanometer-Scale Control of the Electron Injection Layer Morphology through Solvent Processing. *Adv. Mater.* **2008**, *20*, 1565−1570.
(29) Jiang, C.; Zhong, Z.; Liu, B.; He, Z.; Zou, J.; Wang, L.; Wang, J.; Peng, J.; Cao, Y. Coffee-Ring-Free Quantum Dot Thin Film Using Inkjet Printing from a Mixed-Solvent System on Modified ZnO Transport Layer for Light-Emitting Devices. *ACS Appl. Mater. Interfaces* **2016**, *8*, 26162−26168.
(30) Liu, Y.; Li, F.; Xu, Z.; Zheng, C.; Guo, T.; Xie, X.; Qian, L.; Fu, D.; Yan, X. Efficient All-Solution Processed Quantum Dot Light Emitting Diodes Based on Inkjet Printing Technique. *ACS Appl. Mater. Interfaces* **2017**, *9*, 25506−25512.
(31) Kim, B. H.; Onses, M. S.; Lim, J. B.; Nam, S.; Oh, N.; Kim, H.; Yu, K. J.; Lee, J. W.; Kim, J.-H.; Kang, S.-K.; Lee, C. H.; Lee, J.; Shin, J. H.; Kim, N. H.; Leal, C.; Shim, M.; Rogers, J. A. High-Resolution Patterns of Quantum Dots Formed by Electrohydrodynamic Jet Printing for Light-Emitting Diodes. *Nano Lett.* **2015**, *15*, 969−973.
(32) Wang, M.; Zhou, L.; Yu, M.; Liu, C.; Chu, S.; Pan, J.; Lai, W.-Y.; Huang, W. Amphiphilic Conjugated Molecules with Multifunctional Properties as Efficient Blue Emitters and Cathode Interlayers for Inkjet Printed Organic Light-Emitting Diodes. *J. Mater. Chem. C* **2017**, *5*, 7075−7083.
(33) Zhou, L.; Yang, L.; Yu, M.; Jiang, Y.; Liu, C.-F.; Lai, W.-Y.; Huang, W. Inkjet-Printed Small-Molecule Organic Light-Emitting Diodes: Halogen-Free Inks, Printing Optimization, and Large-Area Patterning. *ACS Appl. Mater. Interfaces* **2017**, *9*, 40533−40540.
(34) Cheng, T.; Wu, Y. W.; Chen, Y. L.; Zhang, Y. Z.; Lai, W. Y.; Huang, W. Inkjet-Printed High-Performance Flexible Micro-Supercapacitors with Porous Nanofiber-Like Electrode Structures. *Small* **2019**, *15*, 1901830.
(35) Liu, X.; Yu, Z.; Yu, M.; Zhang, X.; Xu, Y.; Lv, P.; Chu, S.; Liu, C.; Lai, W.-Y.; Huang, W. Iridium(III)-Complexed Polydendrimers for Inkjet-Printing OLEDs: The Influence of Solubilizing Steric Hindrance Groups. *ACS Appl. Mater. Interfaces* **2019**, *11*, 26174−26184.
(36) Bellmann, E.; Shaheen, S. E.; Thayumanavan, S.; Barlow, S.; Grubbs, R. H.; Marder, S. R.; Kippelen, B.; Peyghambarian, N. New Triarylamine-Containing Polymers as Hole Transport Materials in Organic Light-Emitting Diodes: Effect of Polymer Structure and Cross-Linking on Device Characteristics. *Chem. Mater.* **1998**, *10*, 1668−1676.
(37) Cheng, Y.-J.; Liu, M. S.; Zhang, Y.; Niu, Y.; Huang, F.; Ka, J.-W.; Yip, H.-L.; Tian, Y.; Jen, A. K.-Y. Thermally Cross-Linkable Hole-Transporting Materials on Conducting Polymer: Synthesis, Characterization, and Applications for Polymer Light-Emitting Devices. *Chem. Mater.* **2008**, *20*, 413−422.
(38) Aizawa, N.; Pu, Y.-J.; Sasabe, H.; Kido, J. Thermally Cross-Linkable Host Materials for Enabling Solution-Processed Multilayer Stacks in Organic Light-Emitting Devices. *Org. Electron.* **2013**, *14*, 1614−1620.
(39) Zhou, N.; Lee, B.; Timalsina, A.; Guo, P.; Yu, X.; Marks, T. J.; Facchetti, A.; Chang, R. P. H. Cross-Linkable Molecular Hole-Transporting Semiconductor for Solid-State Dye-Sensitized Solar Cells. *J. Mater. Chem. C* **2014**, *118*, 16967−16975.
(40) Huang, C.-F.; Keshtov, M. L.; Chen, F.-C. Cross-Linkable Hole-Transport Materials Improve the Device Performance of Perovskite Light-Emitting Diodes. *ACS Appl. Mater. Interfaces* **2016**, *8*, 27006−27011.
(41) Tang, Y.; Zhuang, J.; Xie, L.; Chen, X.; Zhang, D.; Hao, J.; Su, W.; Cui, Z. Thermally Cross-Linkable Host Materials for Solution-Processed OLEDs: Synthesis, Characterization, and Optoelectronic Properties. *Eur. J. Org. Chem.* **2016**, 3737−3747.
(42) Wei, C.; Zhuang, J.; Chen, Y.; Zhang, D.; Su, W.; Cui, Z. Highly Air-Stable Electron-Transport Material for Ink-Jet-Printed OLEDs. *Chemistry* **2016**, *22*, 16576−16585.
(43) Xing, Z.; Zhuang, J.; Wei, C.; Zhang, D.; Xie, Z.; Xu, X.; Ji, S.; Tang, J.; Su, W.; Cui, Z. Inkjet-Printed Quantum Dot Light-Emitting Diodes with an Air-Stable Hole Transport Material. *ACS Appl. Mater. Interfaces* **2017**, *9*, 16351−16359.
(44) Wei, C.; Zhuang, J.; Zhang, D.; Guo, W.; Yang, D.; Xie, Z.; Tang, J.; Su, W.; Zeng, H.; Cui, Z. Pyridine-Based Electron-Transport Materials with High Solubility, Excellent Film-Forming Ability, and Wettability for Inkjet-Printed OLEDs. *ACS Appl. Mater. Interfaces* **2017**, *9*, 38716−38727.
(45) Xie, L.; Zhuang, J.; Chen, X.; Xie, Z.; He, R.; Chen, L.; Wang, W.; Zhang, D.; Su, W.; Tang, J.; Yan, X.; Cui, Z. 0.7% Roll-off for Solution-Processed Blue Phosphorescent OLEDs with a Novel Electron Transport Material. *ACS Photonics* **2017**, *4*, 449−453.
(46) Xie, L.; Xiong, X.; Chang, Q.; Chen, X.; Wei, C.; Li, X.; Zhang, M.; Su, W.; Cui, Z. Inkjet-Printed High-Efficiency Multilayer QLEDs

https://dx.doi.org/10.1021/acsami.0c01001
ACS Appl. Mater. Interfaces 2020, 12, 13087−13095

Based on a Novel Crosslinkable Small-Molecule Hole Transport Material. *Small* **2019**, *15*, 1900111.
(47) Fabregat-Santiago, F.; Garcia-Belmonte, G.; Mora-Seró, I.; Bisquert, J. Characterization of Nanostructured Hybrid and Organic Solar Cells by Impedance Spectroscopy. *Phys. Chem. Chem. Phys.* **2011**, *13*, 9083−9118.
(48) Suarez, B.; Gonzalez-Pedro, V.; Ripolles, T. S.; Sanchez, R. S.; Otero, L.; Mora-Sero, I. Recombination Study of Combined Halides (Cl, Br, I) Perovskite Solar Cells. *J. Phys. Chem. Lett.* **2014**, *5*, 1628−1635.
(49) Okachi, T.; Nagase, T.; Kobayashi, T.; Naito, H. Determination of Charge-Carrier Mobility in Organic Light-Emitting Diodes by Impedance Spectroscopy in Presence of Localized States. *Jpn. J. Appl. Phys.* **2008**, *47*, 8965−8972.
(50) Nowy, S.; Ren, W.; Elschner, A.; Lövenich, W.; Brütting, W. Impedance Spectroscopy as a Probe for the Degradation of Organic Light-Emitting Diodes. *J. Appl. Phys.* **2010**, *107*, 054501.
(51) Jaramillo-Quintero, O. A.; Sanchez, R. S.; Rincon, M.; Mora-Sero, I. Bright Visible-Infrared Light Emitting Diodes Based on Hybrid Halide Perovskite with Spiro-OMeTAD as a Hole-Injecting Layer. *J. Phys. Chem. Lett.* **2015**, *6*, 1883−1890.
(52) Chulkin, P.; Vybornyi, O.; Lapkowski, M.; Skabara, P. J.; Data, P. Impedance Spectroscopy of OLEDs as a Tool for Estimating Mobility and the Concentration of Charge Carriers in Transport Layers. *J. Mater. Chem. C* **2018**, *6*, 1008−1014.
(53) Juarez-Perez, E. J.; Wuβler, M.; Fabregat-Santiago, F.; Lakus-Wollny, K.; Mankel, E.; Mayer, T.; Jaegermann, W.; Mora-Sero, I. Role of the Selective Contacts in the Performance of Lead Halide Perovskite Solar Cells. *J. Phys. Chem. Lett.* **2014**, *5*, 680−685.
(54) Hauch, A.; Georg, A. Diffusion in the Electrolyte and Charge-Transfer Reaction at the Platinum Electrode in Dye-Sensitized Solar Cells. *Electrochim. Acta* **2001**, *46*, 3457−3466.
(55) Pitarch, Á.; Garcia-Belmonte, G.; Bisquert, J.; Bolink, H. J. Impedance of Space-Charge-Limited Currents in Organic Light-Emitting Diodes With Double Injection And Strong Recombination. *J. Appl. Phys.* **2006**, *100*, 084502.
(56) Burrows, P. E.; Shen, Z.; Bulovic, V.; McCarty, D. M.; Forrest, S. R.; Cronin, J. A.; Thompson, M. E. Relationship between Electroluminescence and Current Transport in Organic Heterojunction Light-Emitting Devices. *J. Appl. Phys.* **1996**, *79*, 7991−8006.
(57) Haverinen, H. M.; Myllylä, R. A.; Jabbour, G. E. Inkjet Printing of Light Emitting Quantum Dots. *Appl. Phys. Lett.* **2009**, *94*, 073108.
(58) Haverinen, H. M.; Myllyla, R. A.; Jabbour, G. E. Inkjet Printed RGB Quantum Dot-Hybrid LED. *J. Disp. Technol.* **2010**, *6*, 87−89.
(59) Jiang, C.; Mu, L.; Zou, J.; He, Z.; Zhong, Z.; Wang, L.; Xu, M.; Wang, J.; Peng, J.; Cao, Y. Full-Color Quantum Dots Active Matrix Display Fabricated by Ink-Jet Printing. *Sci. China: Chem.* **2017**, *60*, 1349−1355.
(60) Xiong, X.; Wei, C.; Xie, L.; Chen, M.; Tang, P.; Shen, W.; Deng, Z.; Li, X.; Duan, Y.; Su, W.; Zeng, H.; Cui, Z. Realizing 17.0% External Quantum Efficiency in Red Quantum Dot Light-Emitting Diodes by Pursuing the Ideal Inkjet-Printed Film and Interface. *Org. Electron.* **2019**, *73*, 247−254.

https://dx.doi.org/10.1021/acsami.0c01001
ACS Appl. Mater. Interfaces 2020, 12, 13087−13095

Supporting information

Realizing 22.3% EQE and 7-Fold Lifetime Enhancement in QLED: via Blending Polymer TFB and Cross-linkable Small Molecule for Solvent-Resistant Hole Transport Layer

Pengyu Tang[1,2,‡], Liming Xie[1,‡], Xueying Xiong[1,2], Changting Wei[1], Wenchao Zhao[1], Ming Chen[1], Jinyong Zhuang[3,], Wenming Su[1,2,*], and Zheng Cui[1,2]*

[1] Printable Electronics Research Center, Suzhou Institute of Nano-Tech and Nano-Bionics, Chinese Academy of Sciences, 398 Ruoshui Road, Suzhou Industrial Park, Suzhou, Jiangsu, 215123, People's Republic of China.

[2] School of Nano-Tech and Nano-Bionics, University of Science and Technology of China, Hefei, Anhui, 230026, People's Republic of China.

[3] Guangdong Juhua Printed Display Technol Co Ltd, Guangzhou, Guangdong, 510700, People's Republic of China.

Corresponding Author:

*E-mail: wmsu2008@sinano.ac.cn

*E-mail: zhuangjinyong@tcl.com

‡(P.T. and L.X.)These authors contributed equally

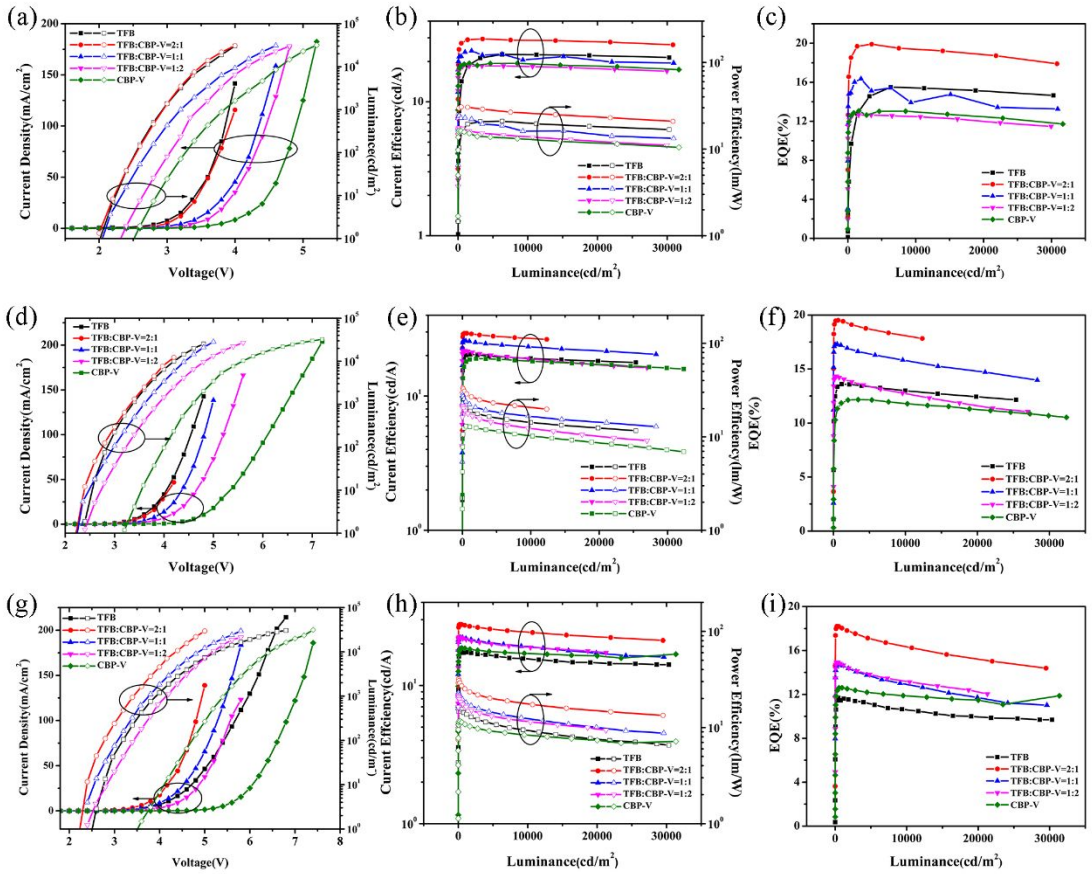

Figure S1 J-V-L (a, d and g), CE-L-PE (b, e and h) and EQE-L (c, f and i) characteristics of the red QLEDs with the HTL thickness of 5 nm (a, b and c), 17 nm (d, e and f) and 28 nm (g, h and i).

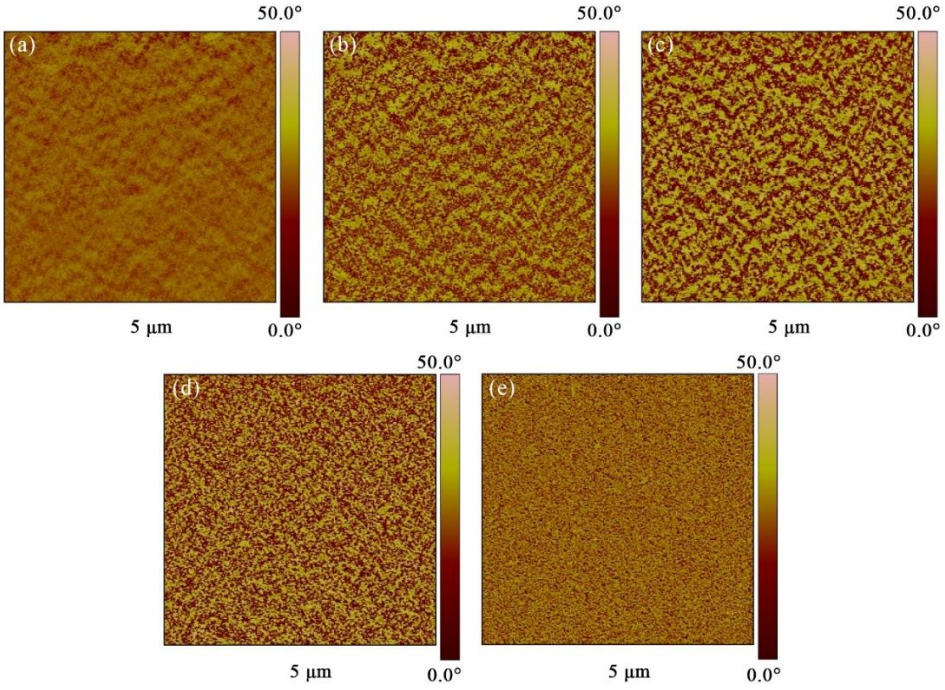

Figure S2 AFM phase graphs: (a) pure TFB, (b) TFB:CBP-V=2/1, (c) TFB:CBP-V=1/1, (d) TFB:CBP-V=1/2 and (e) pure CBP-V

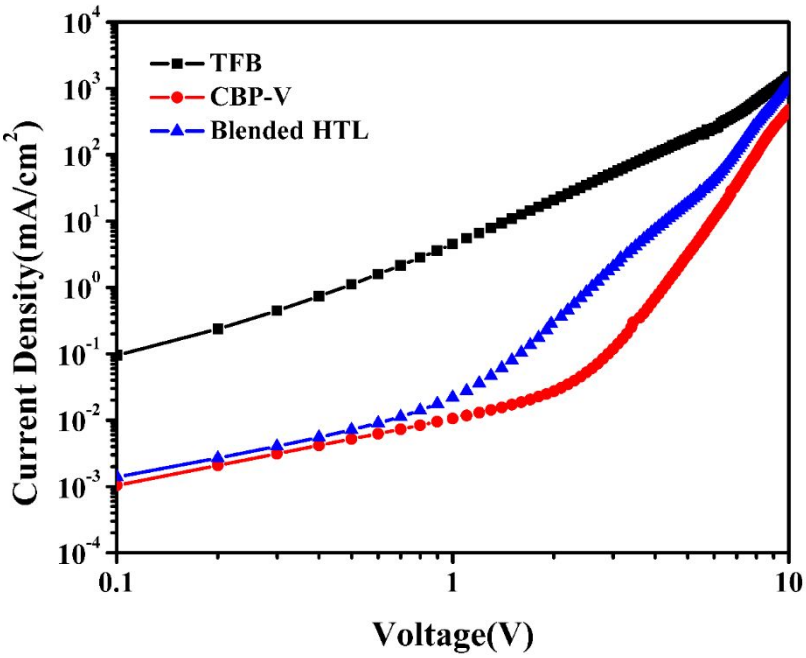

Figure S3 J−V characteristics of the hole-only devices with different HTLs.

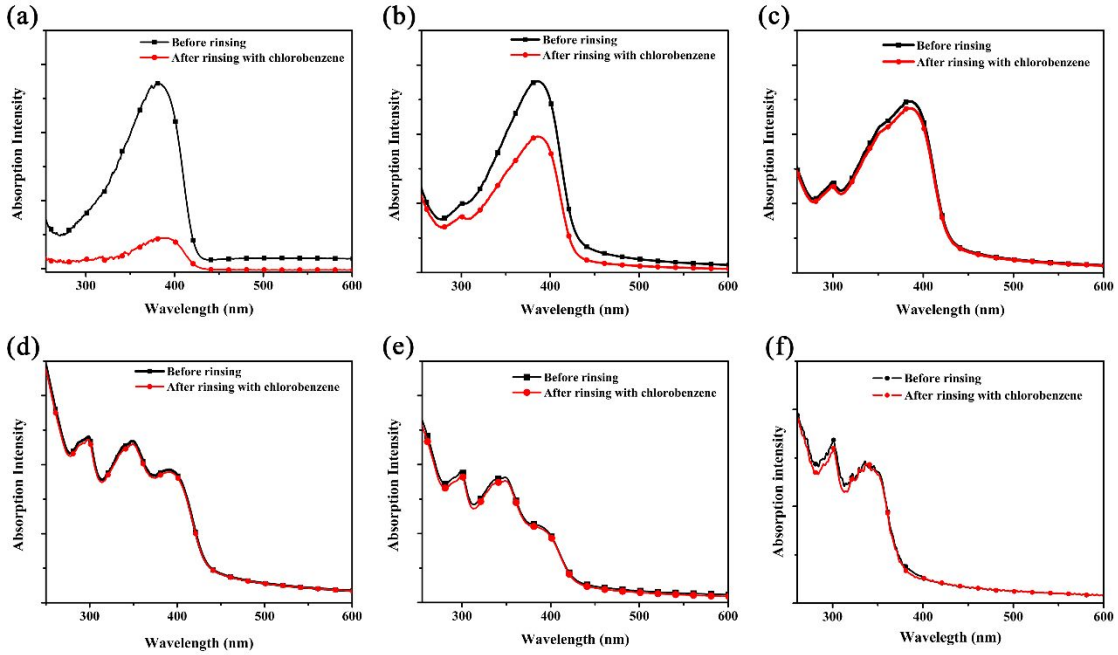

Figure S4 UV–vis absorption spectra of the cured films of different HTLs before and after rinsing with chlorobenzene: (a) TFB, (b) TFB:CBP-V=3:1, (c) TFB:CBP-V=2:1, (d) TFB:CBP-V=1:1, (e) TFB:CBP-V=1:2 and (f) CBP-V

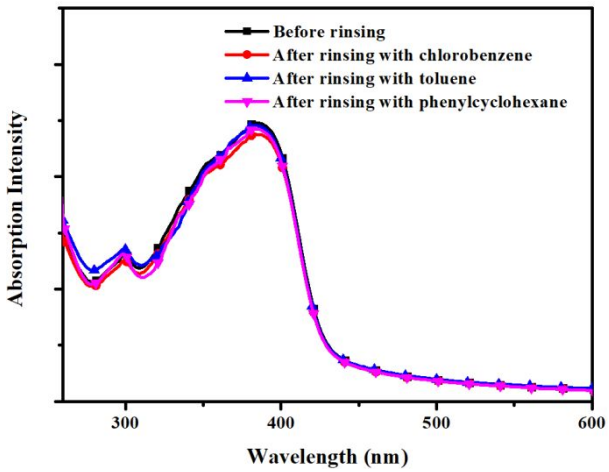

Figure S5 UV–vis absorption spectra of the cured films of blended HTLs before and after rinsing with different solvents.

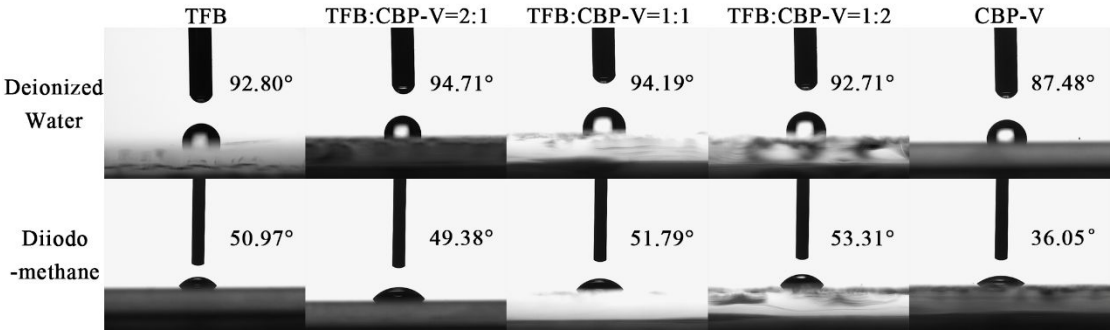

Figure S6 contact angel of deionized water and diiodomethane on different HTLs

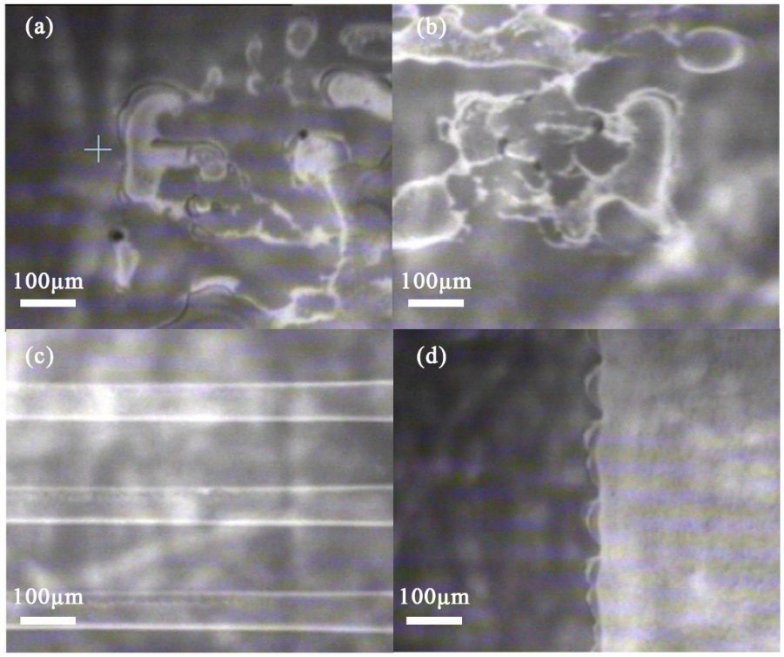

Figure S7 Photographs of square printed on the blended HTLs with the TFB:CBP-V ratio of (a) 1:2 and (b) 1:1. Photographs of (c) lines and (d) square printed on the blended HTL with the TFB:CBP-V ratio of 2:1.

Tablet S1. Summarized performances of the red QLEDs with different HTLs at different thickness

HTL thickness	HTL type	V_T (V)	CE_{Max} (cd/A)	PE_{Max} (lm/W)	EQE_{Max} (%)
5 nm	TFB	2.0	22.57	21.03	15.50
	TFB:CBP-V=2:1	2.0	29.05	30.67	19.91
	TFB:CBP-V=1:1	2.0	24.02	24.18	16.35
	TFB:CBP-V=1:2	2.3	18.50	17.37	12.65
	CBP-V	2.5	19.37	16.40	13.06
12 nm	TFB	2.2	23.41	22.27	15.92
	TFB:CBP-V=2:1	2.2	32.78	36.77	22.31
	TFB:CBP-V=1:1	2.2	24.59	27.50	16.55
	TFB:CBP-V=1:2	2.3	20.28	22.24	13.67
	CBP-V	2.7	19.08	17.51	12.29
17 nm	TFB	2.4	20.39	19.87	13.61
	TFB:CBP-V=2:1	2.2	29.33	33.36	19.47
	TFB:CBP-V=1:1	2.2	25.85	28.00	17.30
	TFB:CBP-V=1:2	2.4	21.77	21.47	14.00
	CBP-V	3.1	18.99	12.96	12.17
28 nm	TFB	2.5	17.44	16.14	11.68
	TFB:CBP-V=2:1	2.2	27.39	31.94	18.21
	TFB:CBP-V=1:1	2.2	22.30	23.17	14.69
	TFB:CBP-V=1:2	2.4	21.78	21.43	14.92
	CBP-V	3.5	18.70	11.66	12.61

Tablet S2 Fitting parameters for the TRPL spectra

Structure	A_1	t_1	A_2	t_2	τ_{ave}
pure QD	0.05	89.08	0.95	12.06	34.27
TFB	0.04	73.70	0.96	8.83	26.45
blended HTL	0.06	75.85	0.94	10.49	30.91
CBP-V	0.95	11.38	0.05	85.71	32.35

The fitting for decay curves is carried out based on a double-exponential function:

$$I = I_0 + A_1 \cdot e^{-\frac{\tau_1 - t_0}{t}} + A_2 \cdot e^{-\frac{\tau_2 - t_0}{t}}$$

where τ_1 and τ_2 represent the decay time constants, and A1 and A2 represent the normalized amplitudes of each component; A1 + A2 = 1. Therefore, the average lifetime of the decay is calculated by:

$$\tau_{ave} = \frac{A_1 \cdot \tau_1^2 + A_2 \cdot \tau_2^2}{A_1 \cdot \tau_1 + A_2 \cdot \tau_2}$$

Tablet S3 Fitting parameters of the Nyquist plots for QLEDs at 3 V

HTL type	R_s (Ω/cm^2)	R_{tr} (Ω/cm^2)	CPE_1 ($S \cdot Sec^n/cm^2$)	n_1	R_{rec} (Ω/cm^2)	CPE_2 ($S \cdot Sec^n/cm^2$)	n_2
TFB	3.758	146.4	3.77E-07	1	1689	1.29E-07	1
TFB:CBP-V=2:1	2.345	152.6	3.53E-07	1	1285	1.55E-07	1
TFB:CBP-V=1:1	3.28	202.1	3.04E-07	1	1235	1.68E-07	1
TFB:CBP-V=1:2	3.345	252.9	3.09E-07	1	1229	2.04E-07	0.99
CBP-V	3.116	275.1	4.30E-07	1	3584	1.79E-07	1

Tablet S4 Contact angels and the calculated surface energy of different HTLs.

HTL type	Contact angel of deionized water (°)	Contact angel of diiodomethane (°)	Surface energy (mN/m)
TFB	92.80	50.97	34.17
TFB:CBP-V=2:1	94.71	49.38	35.44
TFB:CBP-V=1:1	94.19	51.79	33.87
TFB:CBP-V=1:2	92.71	53.31	32.67
CBP-V	87.48	36.05	42.19